REVIEW

The Impact Of Pulse Energization On Electrostatic Precipitation Performance

J.K. Nelson and L. Salasoo

Rensselaer Polytechnic Institute
Troy, New York

ABSTRACT

The operation of utility electrostatic precipitators is described, and recent technology aimed at improving performance is discussed. By considering the detailed physics of the precipitation process, the rationale for the use of pulse energization is advanced. The use of a suite of theoretical models which permits the description of the salient elements of the precipitation process in both space and time is outlined and such a modeling process ia applied to pulse energization. By this means the advantages, shortcomings, and future possibilities are examined in detail and implications for precipitator control are discussed.

1. INTRODUCTION AND REVIEW

Stack gas emissions from utility boilers have been much restricted by the EPA's New Source Performance Standards of 1.29×10^{-11} kg/J (0.03 lb/10^6 Btu) implementing the new Clean Air Act amendments of 1977. It has been estimated that 20% of the electrostatic precipitators (ESPs) currently in utility service in the U.S. will need updating by the end of the decade simply to meet the new emission standard. However, the issue has recently been compounded by concerns about the incidence of acid rain. Acid rain control measures being implemented require reductions in the sulfur content of the coal burnt. While this will undoubtedly provide a reduction in the emission of sulfur compounds, it will also inevitably increase the resistivity of the resulting flyash. In turn, this will increase the incidence and severity of back corona in utility precipitators which will result in substantial reductions in efficiency, making compliance a difficult issue. Although emphasis has been placed on increasing overall efficiency, there is also growing concern about the removal of particles of respirable size. The establishment of a new National Ambient Air Quality Standard for fine particles following the lead taken by New Mexico would probably be difficult to meet with conventional precipitators since, at the Federal total particle emission limit, an ESP will typically allow 20% of the emission to comprise material of less than 2 μm aerodynamic diameter. The efficiency "window" exhibited by conventional precipitators for particulates in the range 0.2 to 1 μm diameter is well documented [1]. Although the charging of particulates in an ESP inherently depends on particle size, it is of utmost importance that any move to increase efficiency is not made at the expense of the capture of particles of respirable size.

Some of the options available for trying to improve precipitator performance are reviewed below. However, the current emphasis is on the upgrading of existing installations rather than the provision of new, more advanced designs. In this context, the application of pulsed or intermittent powering is an attractive proposition since it lends itself to retrofitting. It is about 1/3 of the cost to retrofit pulsing rather than to meet total emission standards by the provision of additional collector surface area. A pulse energization retrofit involves only the addition of a pulse power supply and controls so that the existing hardware can be utilized. Designs which have been advocated vary [2], but in some cases the existing transformer/rectifier sets can also be utilized.

1.1 Physical Background

In its simplest form the ESP may be described schematically by Fig. 1. A central wire is suspended in a duct formed by the collecting plates. When a high voltage (usually negative) is applied to the wire, the convergent electric field created produces a corona region consisting of electrons, photons and ions of both signs. The drift field established between the corona zone and the plate extracts ions of the appropriate sign (negative in the case of a negative wire). These ions interact with the particulates entrained in the gas stream because they are both driven along the field lines (field charging) and are subject to thermal diffusion (diffusion charging). Such interaction imparts charge to the dust which then experiences a force which drives it towards the collecting plate

0018-9367/87/1200-0657$01.00 © 1987 IEEE

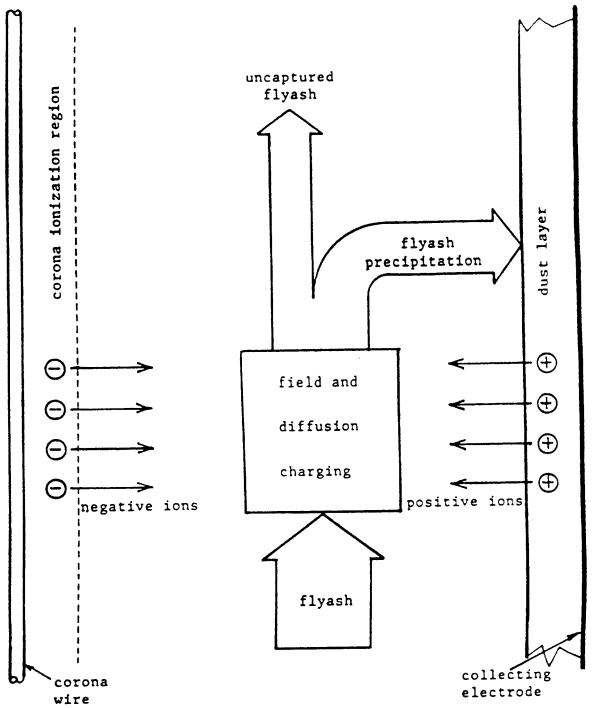

Fig. 1: Schematic showing the fundamental component mechanisms of ESP operation.

where it is held by electrostatic forces until it is removed by mechanical rapping. The essential features of such a precipitator thus involve the processes of corona formation, particle charging, particle migration and dust layer collection. Although at first glance, the dust layer may seem to be a passive and unimportant substrate, this is far from the case. In order to maximize particle charging, conventional ESPs are operated with as high a wire voltage as possible and this results in significant currents flowing in the dust layer. With high dust resistivity, say $>10^{10}$ Ωm, the accompanying voltage drop across the dust layer can result in breakdown of the dust layer, causing material to be reentrained and the injection of copious quantities of positive ions into the drift space, which have a devastating effect on precipitator efficiency. Such a process is commonly referred to as "back corona" but long before currents in the dust layer cause gross breakdown, micro-discharges can occur in the interstices of the particles. This results from the fact that the current is channeled through the points of high contact resistance [3]. The ions so formed "leak" out through the layer to form a back ion flux which severely interferes with charging in the drift space.

The description of the processes of corona, charging, migration and dust layer interactions has been greatly simplified for clarity. In reality these processes cannot be considered in isolation, since all four aspects of ESP performance are interactive. It will become clear from subsequent sections that the main vehicle for this interaction is the space charge created by the charged species in the precipitator.

In recent years there has been increased research on ESP technology which has led to a number of developments and innovations. Much credit for the revival must go to H.J. White whose classic text [4] published in 1963 is still the industry standard. The main thrust of these developments, some of which have been reviewed by Petersen [5], has been to increase the efficiency η of ESPs, often defined by the Deutsch equation as:

$$\frac{1}{1-\eta} = \exp[w(S/H)] \qquad (1)$$

Eq. 1 seeks to express the efficiency in terms of a particle migration velocity w. The ratio of the plate area S to the gas flow rate H is often referred to as the specific collecting area. Although empirical corrections have to be made to Eq. 1 to allow for a distribution in particle sizes and some of the assumptions which underlie it have been called into question, it does nevertheless vividly illustrate the options open to the precipitator designer. It is clear that the dilemma is to avoid the costly increase in the area of the collection electrodes, with the concomitant space penalty, by finding technology to increase the migration velocity w.

Non-pulsed technology options which have been evolved to enhance performance may be divided broadly into three main categories:

1.1.1 Wide Duct Spacing

Traditionally duct spacings in the range *200* to *300* mm have been considered optimum for industrial ESPs for both theoretical and practical reasons. The finding by Heinrich [6] that it was possible to increase efficiency by using a wider spacing led to full-scale experiments which verified an effect that contradicted conventional teaching. It is now recognized that the phenomenon results from the field modifications created by the charged dust particles themselves. The use of wider spacing allows both a higher voltage to be used and provides other benefits such as easier access for maintenance. As a result, renewed efforts have been made to try to optimize the spacing of conventional precipitators, and capitalize on the availability of reliable power supplies having voltages up to *100* kV. There may also be some additional benefits gained from a more uniform current distribution on the collecting electrode which may help to delay the onset of back corona. The impetus to examine wider spacings also has raised the issue of the size and nature of the corona wire used. These are typically *2* to *3* mm in diameter and are often designed to offer field-intensified regions. A better understanding of the underlying mechanisms has resulted in a reexamination of the optimum design of the wire to complement the wider duct spacings.

1.1.2 Two-Stage and Precharging Principles

The application of voltage to a conventional precipitator has to accomplish several functions simultaneously. The resulting field not only creates the necessary ions in the corona discharge but also provides the drift field for charging and the necessary force to maintain the precipitated layer on the collector. If the charging and precipitating functions are separated in a two-stage device then conditions in each stage can be made more appropriate to the respective functions. In particular, the opportunity can be taken to equip the first stage with devices to provide improved particle charging while lower current densities can

be maintained in the second stage collection area. In this respect several innovations have been attempted. The so-called high-intensity ionizer utilizes an array of venturi nozzles with central discharge electrodes to improve the charging capability. A different approach has been taken by the Southern Research Institute [7] in which the wire and plate design has been modified to include a negatively biased third grid elec trode placed in front of the grounded plate to intercept any back ion flux which might otherwise interfere with the charging process. Effective precharging of high-resistivity dust may also be accomplshed by ion bombardment, alternately from two directions, in a device commonly called a "Boxer-Charger" developed in Japan [8]. This is an ingenious arrangement in which a discharge is initiated on a special helical electrode by a high-frequency waveform applied in synchronism with a power frequency voltage applied across the charger. Operation of these devices has been reviewed by Petersen [5] and commercial implications have been estimated by Lagarias et al. [9].

1.1.3 Chemical Conditioning

When the ESP structure is mechanically sound, poor ESP performance in most cases results from attempts to precipitate high resistivity flyash. However, it is estimated [9] that about 150 flue gas conditioning systems have been installed using sodium or ammonium sulfate, sulfur trioxide, or proprietary chemical compounds to alter the electrical properties of the ash [10]. In many instances the low initial cost of chemical conditioning is an attractive short-term measure to maintain compliance. Attempts also have been made to use other additives, such as triethylamine, which is said to improve efficiency by causing agglomeration.

1.2 Pulse Powering

It will be clear from earlier discussion that a major impediment to efficiency improvements is the onset of back ion emission from the dust layer. If improvements in migration velocity are sought by raising the applied voltage then the associated increase in dust layer current enhances the problem of back corona. Fig. 2 schematically demonstrates the way in which pulsing an ESP tries to overcome the problem. A train of pulses, usually superimposed on a dc voltage level, provides a high peak electric field for particle charging. However, the mean collector current in this case depends not only on the peak voltage but also on the pulse duty cycle. In this way the voltage and current can be

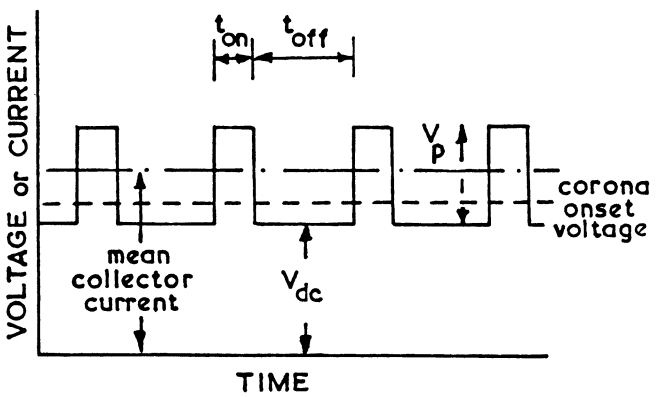

Fig. 2: Idealized pulse waveform showing operating parameters.

decoupled by changing the mark/space ratio of the applied pulses and high charging fields can be established without necessarily incurring the penalty of large dust layer currents. Although pulse powering is not new, there has been increased interest in the technology in recent years [9,11]. If the pulse technology could be optimized, inexpensive retrofitting would allow many installations to operate within the regulations without the need to resort to additional plate area or chemical conditioning.

Until recently, attempts to implement pulse powering have been hampered by the available high-voltage switching technology. However, this has now changed and several schemes have been developed commercially [2,12] with emphasis also being placed on the electrical efficiency so as to reduce the power consumption [2]. Since the cost of running a single *500* MW installation is typically about $100000 per annum, savings in power consumption can amount to considerable sums.

Two strategies have emerged. The first (Ion Physics) involves the use of a narrow pulse width (≃*1* μs) and the other (General Electric, F.L. Smidth) utilizes pulses in the range of *50* μs to *1* ms in width. Inevitably the very short pulses may be applied at greater amplitudes but the product of the ion density and pulse width is reduced. Assessments of such schemes on pilot and full scale tests have been carried out although, as in the case of the test conducted at the Lancing Smith Station of Gulf Power [13], and the measurements conducted at the Beebee Station of Rochester Gas and Electric [14], the circumstances of test often have prevented a good and meaningful evaluation. The experimental use of the narrow pulse scheme at Carolina Power and Light Company's Sutton Station [15], indicated that the collection efficiency could be upgraded from *97.67* to *99.02*%. However, there is now increasing evidence that the performance is critically dependent on the pulse parameters used. Experience has shown that pulse powering can yield performance enhancement factors of *1.2* to *2.0* (migration velocities corrected by the Matts-Ohnfeld method [16]) and factors as high as *2.9* have been recorded for very high-resistivity ash. This wide range justifies the expectation that gains are likely to be made by determining the optimum operating conditions in the pulse mode. The tests at Lancing Smith also indicated a 17% reduction in power consumption for an unoptimized "broad" pulse application.

Japanese experience has shown that pulsing can reduce power requirements by a factor of 5 when compared to conventional dc energization. This again points to the need for optimization to take advantage of the potential improvements. A number of claims have been made for the application of pulse powering to utility ESPs. There is little doubt that they can be substantiated but the evidende suggests that the gains to be made will depend, perhaps critically, on the particular circumstances. It is thus important to examine the sensitivities of these benefits to the electrical parameters of the pulse supply, the geometry and the characteristics of the gas/particulate system. It will be clear from reference to Fig. 2 that, in theory, pulse energization offers the possibility for adjustment not only of the peak voltage but also of pulse width, shape, pulse repetition rate and the level of the dc bias pedestal. However, it can be argued that such total flexibility is not justified with the current state of the art and intermittent pulsing [17] is more cost effective. In this approach control of the

transformer/rectifier set is exercised in such a way as to omit a programmed number of half cycles. By this means a measure of current control, independent of peak voltage, can be achieved.

This contribution seeks to examine the opportunities offered by pulse energization by examining in detail some of the complex physics which underlies the process. By building on a review of the mechanisms, a comprehensive model has been used to permit an understanding of the circumstances most conducive to pulse powering and to allow optimization of control parameters.

2. PHYSICS OF THE PRECIPITATION PROCESS

2.1 Corona Generation

In all ESPs a set of electrodes, typically *2* to *3* mm dia. wires, is energized to produce corona which injects ions into the gas flow. Negative corona is used in an overwhelming majority of applications because it leads to higher operating fields [4].

Negative corona is a pulsating phenomenon occurring at discrete spots or tufts spaced out along the wire cathode [18,19]. Under dc energization, the pulses, called Trichel pulses after the first discussion by Trichel [20], occur at a regular rate from kHz to MHz. Trichel pulses are characterized by a rapid rise time of the order of *1* to *10* ns, followed by a slowly decaying fall lasting of the order of *1* μs. The mean corona current increases with increased applied voltage; however the charge per Trichel pulse varies little with applied voltage, so that the total current is proportional to the Trichel pulse frequency. The current pulse is accompanied by a concurrent burst of light emission caused by deexcitation of electron-excited neutrals; time and space resolved optical studies [21] have clarified many aspects of the Trichel pulse mechanism. Subsequent studies and analyses confirm Trichel's view of a pulse as a fast regenerative ionization phase choked off by the resulting space charge distorted field, followed by a slow relaxation phase.

A cathode with a convergent field, ionization, electron attachment, and cathode secondary emission are necessary for Trichel pulse formation. The converging electric field serves to limit ionization activity to the neighborhood of the cathode, while electron attachment is necessary to quench the temporal development of ionization.

The photoelectric effect is an important source of secondary emission; additionally, positive ion impact to the cathode may also contribute. The rate of excitation of neutral molecules is often considered proportional to the ionization rate. The subsequent radiative deexcitation provides the cathode photon flux, and usually the deexcitation to ionization ratio is factored into the secondary photoemission coefficient.

While the general nature of the Trichel pulse mechanism was discussed by Trichel, several different theories have been presented for the mechanisms which initiate the ionization burst, cause the rate of ionization growth, and choke the ionization burst. Quantitative solution of the describing equations has been necessary to determine which of several possible mechanisms causes the observed behavior. Morrow [22] has carried out a thorough computational study to confirm the accepted theory of Trichel pulses.

The interelectrode space may be divided into two regions or zones: the ionization region close to the cathode where the ionization occurs, and the drift region comprising the space between the ionization region and the anode. In addition, the temporal behavior can be divided into a brief ionization phase of rapid activity in the ionization region, and the relaxation phase when ion movement in the drift region is the dominant effect. In the relaxation phase between Trichel pulses, lasting from μs to ms, a negative ion swarm drifts away from the cathode vicinity towards the anode, leading to an increase in the cathode surface field.

A positive feedback loop is formed by secondary emission, electron avalanches and the resulting photon and positive ion flux at the cathode. The loop gain is the product of the secondary emission coefficient and the Townsend discharge reproduction factor, given by

$$\int_{cathode}^{R:\alpha(R)\,=\,\eta(R)} \alpha(r)\,\exp\left\{\int_{cathode}^{r}(\alpha-\eta)\,ds\right\}dr \qquad (2)$$

which is a rapidly increasing function of cathode surface field. When the loop gain increases above unity, the secondary emission grows, yielding a growing positive space charge accumulation close to the cathode and a cloud of negative space charge at a greater distance. At this early stage of the Trichel pulse, the field near the cathode is Laplacian, but eventually the accumulation of space charge causes significant field distortion, with the field intensity rising close to the cathode and falling further from the cathode. This field redistribution increases avalanche gain, intensifying the rise in ionization, optical output and terminal current.

However, the reduction of field at greater distances from the cathode starts to compress the region of avalanche growth. At this stage, photoemission dominates the secondary emission so that the time lag in the feedback loop is essentially the electron transit time from the cathode to the region of highest ionization activity, of the order of *1* ns. The compression of the ionization region accelerates, producing a front of intense light emission that moves towards the cathode at speeds of about *1* cm/μs (dependent on pressure and cathode radius), leaving a dense, quasineutral plasma with very low field in its wake. When tracked optically, this movement appears like a cathode-directed ionization wave which is stopped short of contacting the cathode by compression of the avalanche region and the resultant reduction in the loop gain. The terminal current and optical output achieve a peak at this time. Now the movement of the positive ions to the cathode becomes significant, possibly initiating a second current peak due to the movement of ion bombardment initiated secondary electrons.

The relaxation phase can be considered to start at this time. The absorption of ions by the cathode reduces the surface field, lowering the terminal current, loop gain and ionization activity. Most of the positive ions are extracted from the plasma and absorbed by the cathode in the first μs although the tail of the swarm may persist several tens of μs. The reduction of cathode field continues for a time of the order of *1* μs; subsequently negative charge movement dominates

and the surface field begins to rise again. Due to the converging cathode field geometry, the negative space charge swarm (consisting chiefly of ions after the first μs, because of electron attachment) moves towards the anode at a low and falling velocity, yielding a low terminal current between Trichel pulses.

As Sigmond [23] observes, the range of time scales spans many orders of magnitude: from sub ns electron transit times from cathode to the plasma in the ionization phase, through *0.1* to *1* μs for pulse quenching by positive ion movement, to *10* μs to *1* ms for the recovery of cathode field; distance scales vary as well from *10* to *100* μm scaled structure in the ionization phase, to the *0.03* to *0.3* m electrode separations.

2.2 Particle Charging

Two important effects bring ions from a surrounding ion swarm to the surface of a particle entrained in the gas flow [4]: drift along field lines ("field charging") and random thermal motion ("diffusion charging"). All ions incident on the particle surface are usually absorbed.

The derivation of the rate equations for field charging of a spherical particle is direct [24]. The field from a sphere of diameter d with charge Q is superimposed on the perturbed field from introducing the same sphere (uncharged) with dielectric permittivity K into a uniform applied field E_o. When $|Q| < Q_s$, the particle surface is divided into two portions, according to whether field lines enter or exit the surface. Q_s is the particle saturation charge given by

$$Q_s = \frac{3K}{K+2} \varepsilon_o \pi d^2 E_o \qquad (3)$$

The particle charges up to $-Q_s$ in the presence of negative ions with a time constant

$$\tau_f = \frac{\varepsilon_o}{b_n \rho_n} \qquad (4)$$

The important features of field charging are that Q_s varies as $E_o d^2$, while the charging rate is proportional to the charging ion density.

The random thermal motion of the ions causes diffusion charging where energetic ions surmount the electrostatic potential barrier to reach the particle surface. When there is no applied field, the following diffusion charging rate equation for negative ions is derived [4]:

$$\frac{dQ}{dt} = \frac{\pi d^2 c \rho_{n^-}}{4} \exp\left[\frac{Qe}{2\pi\varepsilon_o dkT}\right] \qquad (5)$$

where c is the mean ion thermal speed. Mizuno [25] integrates this equation from zero initial charge:

$$Q = -Q_d \ln[1 + t/\tau_d] \qquad (6)$$

with the diffusion charging constant given by

$$Q_d = 2\pi\varepsilon_o dkT/e \qquad (7)$$

and the diffusion time constant given by

$$\tau_d = -\frac{8\varepsilon_o kT}{dc\rho_n e} \qquad (8)$$

Clearly there is no maximum charge, but particle residence time in the ESP imposes a practical limit. The charge after a constant time interval will be proportional to $d.\ln[1+Cd]$.

When there is an applied field combined with the thermal diffusion, no closed-form solution is available. In the conditions of field normally encountered in ESPs, diffusion charging effects become significant for particles smaller than about *1* μm.

The Field Assisted Diffusion (FAD) charging model [26] combines these effects by segregating the particle surface into three regions (see Fig. 3). Region I corresponds to the field charging region and region III

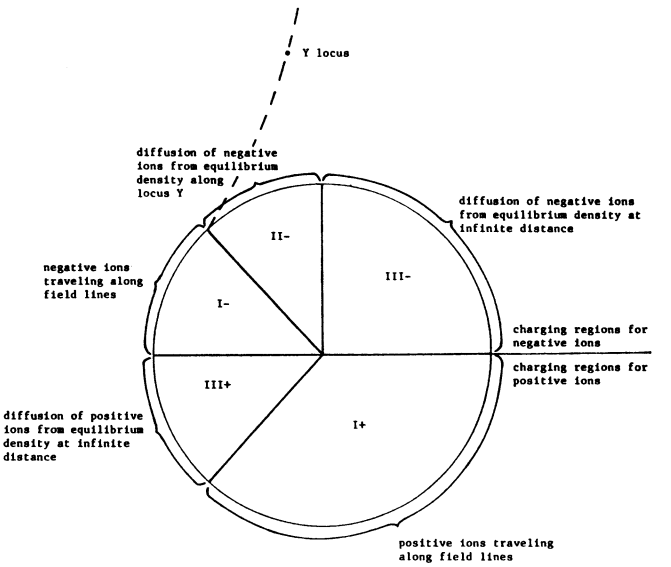

Fig. 3: Classification of particle surface regions in bipolar field assisted charging model.

intercepts a diffusion ion flux corresponding to the particle potential barrier (with zero applied field). A third, intermediate, region II is introduced on the particle surface, where the diffusive ion flux corresponds to a varying potential barrier of intermediate value, to reflect the effect of the applied field in bringing ions close to the particle. The resulting charging rate equation has no closed-form solution, but can be integrated numerically. In the limit of large particle size and high field, the FAD equations approach the field charging result. It is demonstrated that the FAD equations describe an independent set of particle charging measurements [27] quite well.

2.3 Particle Migration and Capture

Once charged, the entrained particles are driven to the collecting electrode by the electric field. The migration velocity w of a charged spherical particle is given by balancing the electrostatic force with Stokes' Law viscous drag [4]:

$$w = \frac{QE}{3\pi\mu d}\left(1 + \frac{2\alpha\lambda}{d}\right) \qquad (9)$$

where μ is the gas absolute viscosity and $2\alpha\lambda/d$ is the Cunningham correction factor which accounts for small-particle behavior when d becomes comparable to λ, the

mean free path (parameter $\alpha=0.86$ for air). The particle acceleration time constant is low compared to migration time for the particle sizes encountered in ESPs, so that inertial effects may be neglected.

ESP gas flow is turbulent, which introduces a mixing action that opposes the migration to the collector. With turbulence present, Eq. (9) gives w relative to the local flue gas velocity; however the equation will not apply with the ESP wall as reference. An effective migration velocity is deduced from efficiency using Eq. 1. The turbulent gas flow can be resolved into a time-independent component, and a fluctuating component with zero mean due to turbulent eddies. The fluctuating component increases the particle diffusion rate through the gas, which may be described by a turbulent or eddy diffusivity, introducing a Fick's Law diffusion term into the particle density equations [28].

In addition, gravitational settling forces act on entrained particles. While White suggests that settling is unimportant for particles smaller than 0.1 mm, others [29] find that up to 50% collection efficiency may be ascribed to nonelectrical effects, including gravitational settling.

Eqs. (3), (7), and (9) show that the particle charge and migration velocity are affected by particle size. If Q_s is substituted into Eq. (9), it can be seen that w is proportional to d, so that larger particles are collected preferentially. Therefore calculations of ESP efficiency must account for the particle sizes, which usually conform to a log-normal distribution [4].

2.4 *Rapping and Reentrainment*

Once particles have been collected on the anode, they are usually removed by rapping, where a mechanical impact is applied to the collector to dislodge caked particulate which falls into hoppers below. The caking qualities of the particulate, the cake thickness and rapping techniques, all combine to affect the efficiency of this transfer. Usually some portion of the precipitated material is reentrained into the gas flow, reducing ESP efficiency. In addition, high gas velocities will scour the precipitated dust layer, also causing reentrainment. Empirical studies show that gas speeds should be kept below 1.8 m/s to curb this effect.

2.5 *Particle Layer Electrical Effects*

The precipitated particulate layer presents a nonlinear resistance to the flow of corona current. A model of the layer as an array of compressible spheres [3] suggests that behavior around the interparticle contacts causes major differences in electrical properties compared with homogenous bulk material. Electrocompression due to current flow through the contacts increases contact area, producing a nonlinear resistivity. Flyash particles have two modes of conduction: volume conduction through the particle bulk, and surface conduction facilitated by the absorption of moisture or other molecules such as ammonia derivatives or sulfate ions [30-33]. The resistivity of a flyash layer is strongly temperature dependent, with lower temperatures (up to 50 to 100°C) usually dominated by surface conduction and higher temperatures (above 100 to 150°C) by volume conduction. Rising temperature decreases surface conduction but increases volume conduction, so the observed resistivity of a flyash layer usually peaks at 50 to 150°C at values of 10^7 to 10^{12} Ωm. The voltage drop across the layer affects corona by reducing the voltage available for corona generation.

At typical ESP collector current densities of 10^{-4} to 10^{-3} A/m^2, layer resistivities of 10^9 to 10^{10} Ωm lead to average layer fields of 1 MV/m, approaching the bulk strength of air. A partial breakdown in the layer, called back corona, occurs at these current levels for high resistivities (usually 10^9 Ωm or higher). The average field is below the gas breakdown stress, but field intensification around the interparticle contacts is believed to cause localized microdischarges in those regions [34]. Some of the positive ions generated by the ionization in the microdischarges penetrate into the gas space and degrade ESP operation by aggressively discharging the negatively charged entrained particles. The flux of positive ions to entrained particle surfaces introduces extra terms into the charging rate equations. With field charging, Q_s is degraded to Q_s'

$$Q_s' = \frac{1 - \sqrt{\alpha}}{1 + \sqrt{\alpha}} Q_s \tag{10}$$

with the backflux ratio

$$\alpha = j_p/j_n = \frac{b_p \rho_p}{b_n \rho_n} \tag{11}$$

Masuda [35] demonstrates that $\alpha=1\%$ yields an 18% degradation in Q_s.

In addition, the positive ions of back corona act to increase the field around the corona wire, intensifying the corona. The ESP terminal I/V characteristics are perceptibly different in the presence of back corona.

2.6 *Sparkover*

ESP operating voltage is ultimately limited by sparkover between the electrodes. Sparkover causes a temporary cessation in ESP action by discharging the electrodes, possibly discharging entrained dust with positive ions, and causing reentrainment of collected dust. ESP power supplies are designed to limit the intensity and effects of sparkover [36].

In convergent electrode configurations such as in ESPs, sparking is understood to consist of an anode-directed ionization streamer which leaves electrons in its wake and prepares the path for a returning cathode-directed streamer. The detailed methods of streamer propagation are not completely understood. The most controversial question is the source of electrons ahead of the anode directed streamer head. Proposed mechanisms include photoionization [37], or ionization by a shock wave of high temperature electrons [38]. Studies of sparkover mechanisms in ESPs have not been reported, though the sensitivity to flyash properties has often received comment [39].

2.7 *Electron Charging*

In air and flue gases near atmospheric pressure, the overwhelming majority of corona-generated electrons attach to become negative ions within 5 to 10 mm of the cathode. Thus electrons are significant in only a small portion of the ESP total volume. At reduced pressures electrons travel further before attachment and for ESP electrode separations as low as 25 mm [40], electrons may become significant in the charging of particles. Experimental evidence of electron charging has been reported [40,41]. The much higher mobility, temperature and thermal speed of electrons compared to

ions can be expected to lead to increased charging rates.

2.8 *Interaction of Pulsed Energization With ESP Physics*

The most obvious effect of pulsed energization is on corona generation. For medium and long pulses (*>10* μs), the Trichel pulse ionization phase processes are much faster than the applied voltage pulse, so that individual Trichel bursts are expected to be little different from the dc case. However, the rising edge of the applied voltage speeds up the cathode surface field recovery, so that many Trichel pulses may form on the rising edge. For short applied voltage pulses, the steepness of the leading edge can increase the Trichel burst intensity. For all lengths of voltage pulse, most of the corona activity will occur on the leading edge. The corona produces a dense negative ion swarm which drifts to the anode.

The applied voltage pulse boosts the applied field in the gas space, enhancing particle charging. Even when the energizing pulse has decayed, an increased charging field due to the dense negative ion swarm persists until the swarm has passed by the point of interest. The increased electric field will also serve to increase the electrostatic force on charged particles and enhance their migration towards the anode.

The negative ion current to the collected dust layer will come in waves. However, for resistivities of 10^{10} Ωm or more the *RC* time constant of dust layer resistivity and permittivity is so high (*0.2* s or more) that the layer conduction is smoothed out, and any back corona activity is expected to have an average intensity changing with same time constant.

Finally, pulsing has been observed to improve corona uniformity by driving a larger proportion of the cathode surface into corona than with dc energization alone [42]. The localization of negative corona into tufts is believed to be due to variations in secondary emissivity over the cathode surface. Only the regions with the highest values are active when dc energization is used. The leading edge of the applied pulse raises the Townsend reproduction factor above *1* even for those cathode regions that have secondary emission coefficients well below the maximum values so that the regenerative corona processes of Section 2.1 take place over a larger part of the cathode.

3. MODELING OF PULSED PRECIPITATION

As discussed in the introduction, several different mechanisms have been advanced to account for the observed increases in ESP efficiency caused by pulsed precipitation. Most of the ESP processes are understood and have been characterized mathematically. A computer model facilitates the study of the sometimes complex interactions of pulsed precipitation, permitting a more thorough study of more variables than is possible through laboratory experiments and field studies. As pulsing looks to transient effects to enhance particle charging and control corona, these processes at least will have to be modeled dynamically.

3.1 *Corona*

Almost all published corona models for ESP study (e.g. [43]) are steady state, treating only negative ion flow in the drift region. Since ionization is not modeled explicitly, assumed boundary conditions of cathode surface electric field or ionization current are necessary. Judicious adjustment of these boundary conditions permits quite good agreement to be obtained with experimental measurements of terminal current with dc powering. Such models are not capable of predicting ESP behavior from material properties and arbitrary ESP dimensions. However, calibration by experimental measurements does allow prediction of dc operating behavior. For adequate study of ESP performance under pulsed energization, the behavior in the ionization region must be addressed.

Because the Trichel pulse behavior in the ionization region is emphatically transient in nature, successful quantitative analysis has been forced to follow the time evolution of the ionization burst. This approach required significant amounts of computer calculation. Such an approach has been used to simulate the development of a gas discharge between parallel plates [44-47], and also to produce a definitive study of the Trichel pulse ionization phase in a point-plane geometry [22]. Mengozzi and Feldman [48] describe a one-dimensional time-dependent model of Trichel pulse development in a cylindrical geometry. Several simplifications have been made to avoid large scale computation, and the study only considers *2* to *5* μs energization pulses producing a single ionizing burst.

In studying the full range of pulse widths that has been proposed, from μs ("narrow pulse") through *100* μs ("medium pulse") to ms ("broad pulse"), it is necessary to have the capability to model multiple Trichel pulse formation during the applied voltage pulse. It has been shown that while a *1*-D dynamic model is adequate to describe the ionization phase of a Trichel pulse, one spatial dimension is insufficient for adequate representation of the cathode surface field recovery and the drift of the negative ion swarm [49].

A *2*-D model such as the one outlined in the following [50] gives good results with both dc and pulse energization. The behavior of corona tufts spaced at intervals along a dc or pulse-energized round wire cathode coaxially set inside a tubular anode is obtained. The model features a non-uniform *2*-D grid with adaptive time step and regridding abilities. A pattern-recognizing driver, which monitors the corona simulation progress, obtains computational economies by suppressing certain physical processes at times when they become unimportant. Arbitrary voltage waveforms can be applied and the model computes the time varying values of terminal current, as well as electron and ion density and electric field profiles in the ESP. The secondary electron emission due to ions and illumination is modeled, together with positive ion injection from back corona in the precipitated dust layer. Ionization and attachment are treated, with electrons and ions drifting at velocities derived from the time varying field profile. The latter is obtained from the space charge distribution, the applied cathode voltage and the dust layer surface voltage profile due to the anode dust layer resistivity and permitivity. Experimental data on the extent and spacing of corona tufts is necessary, and can be obtained from optical measurements such as that outlined in [42].

For further computational economy, use is made of the observation that the characteristics of Trichel pulses for a particular apparatus are relatively constant except at very high currents. The ionization phase of the pulse, lasting around *1* μs, is computed once, and superimposed on the simulation whenever the cathode conditions are ripe for Trichel pulse formation. The combination of techniques permits the

computation of behavior over a wide range of time scales, from the subnanosecond phenomena during the ionization wave to the effect of dust layer relaxation times of *0.01* to *0.1* s. Comparisons with experimental measurements using both dc and pulse energization [40, 51] confirm the efficacy of this approach.

3.2 Particle Charging

In modeling the effect of pulsed energization on particle charging, the effect of the time-varying applied field and ion density environment of the particle must be considered. The charging Eqs. (3) through (5) presumed a quasi-steady-state environment where the ion densities have equilibrated, and the experimental verifications of these equations have been carried out under such conditions. It has been recognized [52], that under rapidly changing applied conditions, nonequilibrium depletion zones may form around the particle, degrading charging efficiency. However, it is shown that for energizing pulses superimposed on a dc base voltage, this effect is minor. Therefore, in the model described here, the equilibration processes have been considered to occur much more quickly than the particle charging dynamics, so that the FAD rate equations are applicable using time-varying applied field and negative ion density. In a bipolar environment, complementary terms are added to the FAD equations to account for charging by the back corona generated positive ions, as indicated in Fig. 3.

The particle charging environment varies spatially and, in general, locations closer to the cathode are more effective at charging. However, particle migration to the anode removes particles from the vicinity of the cathode. Thus, to model the overall effectiveness of particle charging, the spatial variation of particle density is required, necessitating a close coupling to the particle migration model.

3.3 Migration and Efficiency

While analytical solutions may be derived for the particle distribution in an ESP due to electric forces and finite turbulent diffusivity in a parallel plate [53] or a coaxial [50] geometry, such solutions are valid only for uniformly charged particles in a Laplacian field. Approximate numerical methods are necessary once space charge distorted fields and spatially varying charging are introduced. Such a model has been incorporated into the comprehensive pulsed ESP model, where the behavior of a coaxial ESP is computed using a *2*-D mesh. The effects of the time-varying field and ion profiles generated by the *2*-D corona model are utilized to generate particle charging and migration data in lookup table form. Particle flow is introduced at the ESP inlet and the particle continuity equations (combining the effects of migration, turbulent diffusion and translational gas flow) are integrated in time, together with the particle charging effects, until a steady state is achieved.

The presence of particle diffusion ensures that particles do not travel a unique path to any particular ESP location. This combines with the spatially varying charging rates to require the description of particle charge as a particle charge distribution. It should be noted that measurements of particle charges from ESPs always indicate a distribution of charges rather than any unique value [54,55]. A novel stochastic scheme is introduced in the model to characterize the distributions in terms of moments and to formulate the behavior of the moments with respect to charging, migration, diffusion and gas flow. The computed particle density profile in the ESP is combined with the steady gas axial velocity profile to yield particle fluxes at the ESP inlet and outlet. These give the computed efficiency, or penetration $P=(1-\eta)$ of the ESP. The model, operating in combination with the pulsed corona model has been verified in comparison with experimental ESP measurements [28,40].

3.4 Dust Layer Effects

Modeling of dust layer resistance should consider its nonlinear nature, since anode current densities in an ESP may vary by more than an order of magnitude over different locations [56]. The sphere array model [3] yielded an approximate power law relationship and experimental measurements of flyash characteristics [57] also show a power law resistance characteristic. The model used here [51] follows earlier models [58] in considering the positive ion flux from back corona to be controlled by the conduction current through the layer. A two-part j_p vs j_n (positive vs negative ion current) characteristic is used, giving a threshold j_n and a constant slope above the threshold. Experimental measurements [57] can give suitable threshold and gain values. The resistance and back corona properties are integrated together with dust layer permittivity into the pulsed corona model as the anode boundary condition.

3.5 Discussion

While the bulk of industrial ESPs has a wire-duct geometry, this geometry has not been used in the above models because treating it would require *3*-D spatial modeling of corona, which could become too expensive computationally. Much of the relevant physics occurs in the ionization zone, remote from the anode, so that the effect of the particular anode shape - flat or cylindrical - will be secondary to the ionizing processes. The drift region field and ion profiles will be affected more by the anode geometry, although no new modes of corona behavior are expected. In the future it could become necessary to model the drift region of wire-plate geometry in the *3*-D.

As discussed elsewhere [50], it may be computationally advantageous to replace the two-dimensional Eulerian (stationary grid) model of migration by a one-dimensional Lagrangian (moving grid) model by neglecting axial diffusion effects and any boundary layer. In such a formulation, a flow surface would be tracked from ESP inlet to outlet with time and space dependent charging, migration and diffusion being calculated on this moving mesh.

A few of the parameters in these models must be determined empirically or estimated. The secondary ionization coefficients required for corona modeling are known to vary dramatically with cathode material and surface condition, but studies have shown that the quantity of ionization has a low sensitivity to these factors. Corona tuft size and spacing should be obtained from experimental measurements. Leonard et al. [53] discuss the calculation of appropriate eddy diffusivity values in ESPs. While there are diffusivity formulas for fully developed duct flow [59], the increased turbulence due to eddy generation by poorly engineered duct geometry can increase the eddy diffusivity to much higher values. The positive ion emission characteristic of back corona has been measured experimentally, but the resolution of these measurements does not permit the recognition of low levels of

positive ion generation which are still significant for particle discharging.

4. EFFECTS OF PULSING

Once a model of pulsed precipitation has been established, a wide range of studies can be undertaken to identify the effects of pulsed energization and their influence on efficiency. Here the benefits of modeling become apparent: most experimental laboratory or field studies are very limited in the variables measured (terminal current and voltage, collection of efficiency over the whole inlet particle size distribution), the precision and reproducibility of measurements, and vulnerability to interference from other uncontrolled process variables. Studies have been carried out [50, 51,60] using the combined model suite described above. Most of the following discussion is based on these studies, which have yielded the illustrative examples. While the effects on ESP efficiency will not be ignored, the more fundamental insights to be gained by discussing the effects on physical processes will be emphasized in this section.

4.1 Corona

The ionizing phase of a Trichel pulse lasts for *0.1* to *1* μs under normal ESP conditions, so that sub-microsecond fast pulses [19] of the type illustrated in Fig. 4 affect the progress of the ionization phase, while the "medium" and "long" pulses do not. Fast pulses will raise the field over the bulk of the cathode surface to high values. At high work function areas (which under dc conditions have insufficient secondary emission coefficients for corona tufts to form), the high avalanche gain for secondary electrons overcomes the low secondary emission coefficients to produce regenerative ionization, and corona will cover most of the cathode surfaces in contrast to the tufting observed under dc energization. When the pulse rise time is more than *1* to *2* μs, several Trichel pulses will form, with each Trichel pulse producing a similar amount of ionization per tuft as for dc. The corona becomes less homogeneous, with fewer Trichel pulses forming at high work function cathode areas.

For fast and medium length pulses, Figs. 4 and 5 of ESP terminal current show that most of the ionization occurs on the rising edge of the energizing pulse (*-45* kV peak on *-22.5* kV bias); with the medium, *100* μs energizing pulse, some Trichel pulses form at the energization peak. There is no ionizing activity during the fall time because the falling voltage and the shielding of the negative ion swarms combine to keep the cathode surface field too low for regenerative ionization.

The amount of ionization-produced negative charge per tuft must be sufficient to force the cathode surface field to remain below the corona inception field at the peak applied voltage. For fast and medium energizing pulses, there is insufficient time for the negative ion swarm to drift far enough away from the cathode to reduce its shielding effect at the wire surface, and therefore the amount of ionization produced by pulses below about *100* μs depends strongly on peak voltage and only weakly on pulse width.

When longer pulses such as the *1* ms pulse producing the response of Fig. 6 are considered, negative ion drift during the pulse (Fig. 7(a) and (b)) is significant, and the above strictures no longer hold. Ionization activity continues during the pulse peak and a lesser amount may take place on the falling edge. The

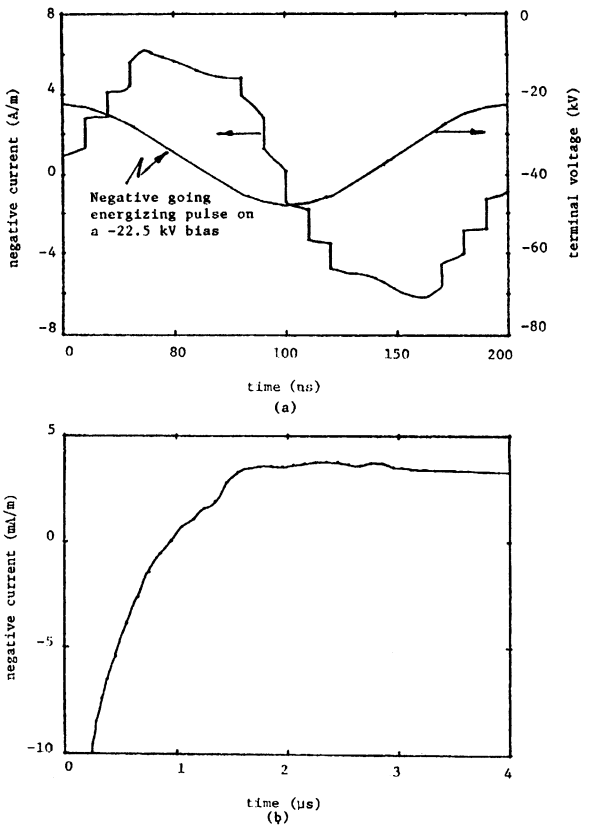

Fig. 4: (a) Fast 100 ns energizing voltage pulse (on a -22.5 kV bias) and current response per meter of wire on a nanosecand time scale. (b) Current response on a microsecond scale. 2.77 mm wire, 229 mm tube, 444 K flue gas.

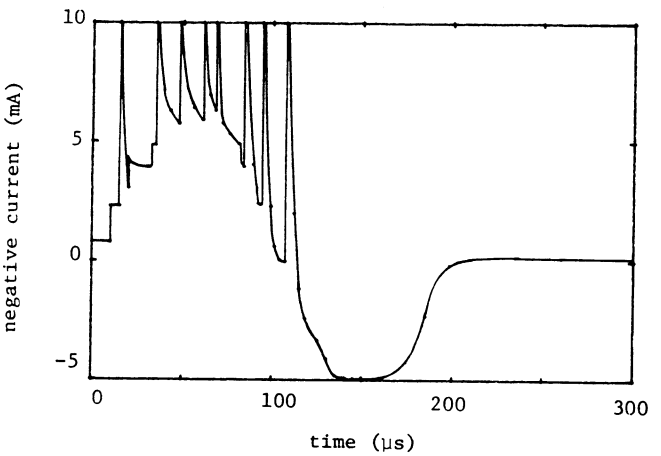

Fig. 5: Response per meter corona wire to medium 100 μs energizing pulse. Other parameters as Fig. 4.

space charge produced per energizing pulse begins to rise with pulse width, though pulse amplitude remains the most important factor in controlling the space

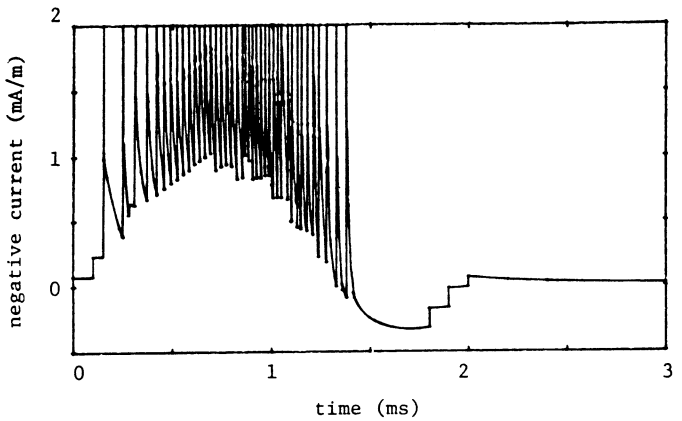

Fig. 6: Response per meter corona wire to long 1 ms energizing pulse. Other parameters as Fig. 4.

instance, Figs. 8(b) and 8(d) show that at $(r,z)=(0.05$ m, $0.$m$)$ and $t=220$ μs for the *100* μs pulse (when the energizing pulse has passed), the negative ion density of about 4.0×10^{14} m^{-3} ($\log 2\pi r N_n = 14.1$) coexists with a field of about *210* kV/m. At the time of the pulse peak ($t=100$ μs), the field is enhanced to *340* kV/m at the same location, (see Fig. 8(c)) but the bulk of the negative ion density (Fig. 8(a)) has not moved far enough radially to exploit this value. *1* ms energizing pulses last long enough for the particle charging field enhancement by the energizing voltage to cause significant improvement in particle charging as seen in Fig. 7(a) which shows that at $t=1.0$ ms (the energizing pulse peak) and the (0.05 m, 0m) location, the negative ion density of 6.3×10^{14} m^{-3} coexists with a *370* kV/m field (from Fig. 7(c)). An interesting feature in Fig. 7(d) is the "trough" with field below *100* kV/m located at $r=0.06$ m, at $t=2.2$ ms, after the energizing pulse has passed. The trough is caused by the combination of the negative ion swarm approaching the anode (at $r=0.11$ m, and the applied *22.5* kV terminal voltage.

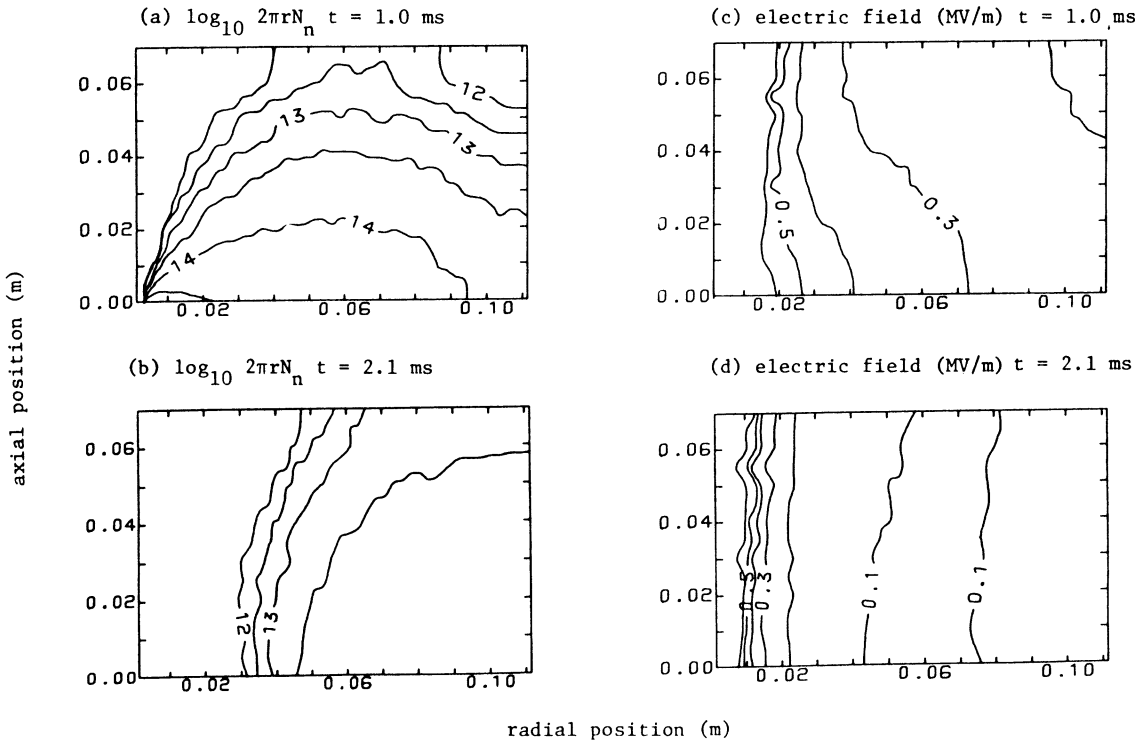

Fig. 7: Negative ion density and electric field profiles from 1 ms pulse.

4.2 Charging

Enhancements in particle charging require increased field levels to occur concurrently with negative ion density. In the region adjacent to the cathode, fields are very high and high peak ion densities are found for fleeting periods, and only a minority of particles enters this small portion of total ESP volume. With fast and medium pulses, negative ions do not move far enough into the gas to have a significant effect on particle charging during the energizing pulse as can be seen in Fig. 8. However, even after the energizing pulse is over, the resulting negative ion swarm enhances the field between the middle of the swarm and the anode. This effect occurs for pulses of all durations. For

For fine particles, diffusion charging mechanisms (which are less sensitive to applied field) are significant. Because increased field is the agent which enhances particle charge with pulse energization, such enhancements are less for fine particles. This effect can be seen in Fig. 9, indicating the enhancement of mean particle charges at the ESP exit for dc and pulsed energization (no back corona effects).

Pulsing significantly enhances charge for particles over *1* μm, with the *1* ms pulse clearly producing higher charges for particles over *4* μm than the other pulses. If purely dc energization is used at a higher level, it is clear that the particle charges are raised equally for all sizes.

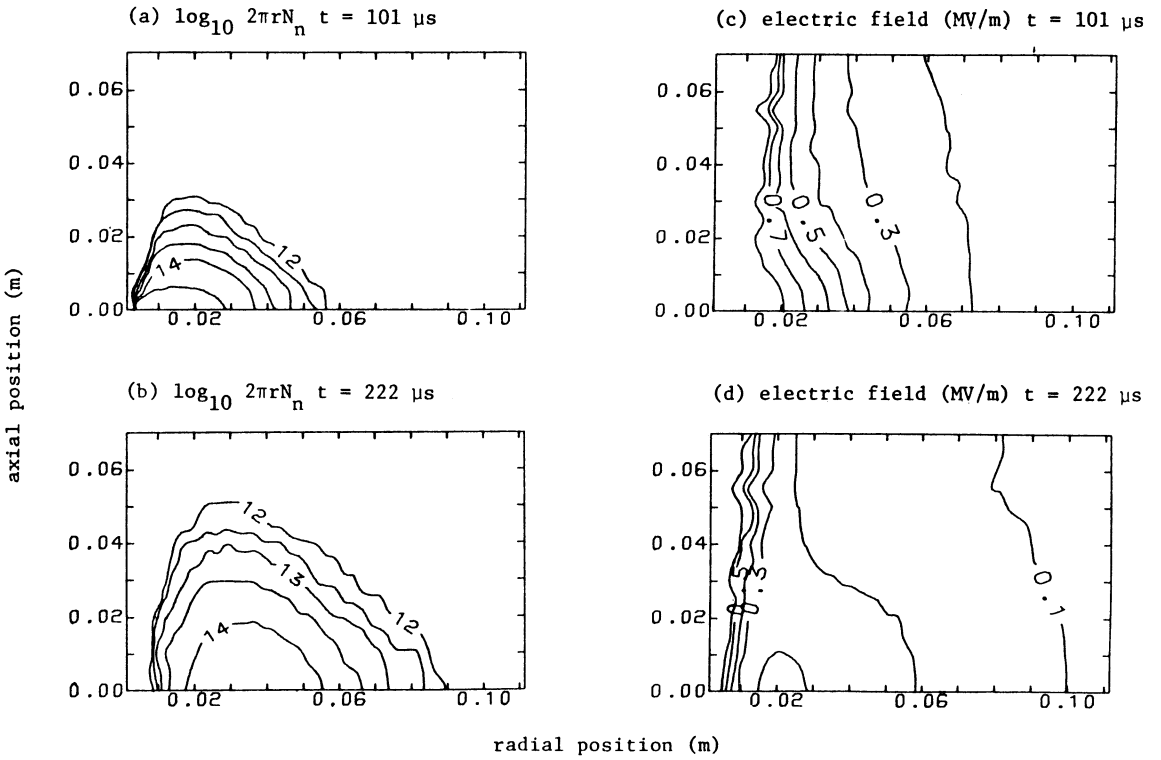

Fig. 8: Negative ion density and electric field profiles from 100 μs pulse.

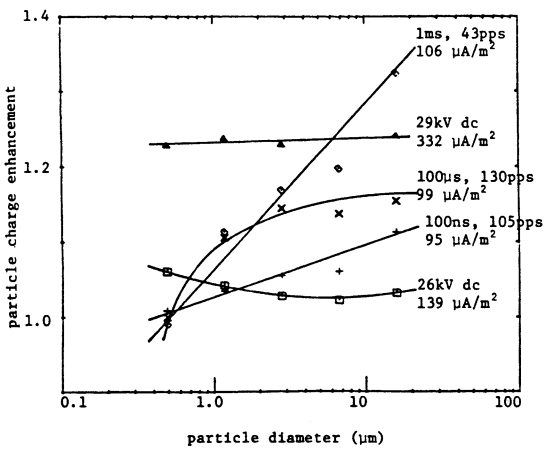

Fig. 9: Enhancement of mean particle charge relative to 25 kV dc energization. 8.23 m long ESP, 1.75 m/s core gas velocity, 22.5+22.5 kV pulses.

4.3 Particle Transport

Pulsing raises the time-averaged field, enhancing particle migration velocity. As mentioned in the previous Section, the effect of negative ion space charge in increasing ESP fields persists after the direct effect from the energizing pulse. Therefore, short and medium pulses below about *100* μs, which produce similar amounts of ionization for the same peak voltages, yield similar time averaged ESP radial fields, while for longer pulses, increasing pulse width begins to increase the average radial fields. Improvements in w accrue from the enhanced field.

4.4 Back Corona and Positive Ion Flux

The uniformity of anode current density depends on the corona tuft distribution, with the maximum density occurring opposite the cathode tufts. Therefore back corona intensity varies over the dust layer and it is quite possible for only part of the layer to be in back corona. This is particularly the case for a duct-type ESP. The increased negative corona uniformity for narrower pulses permits somewhat higher mean anode current densities before the back corona threshold than permitted by dc energization. The effect of back corona on particle charge and consequently migration velocity is seen in Fig. 10 which shows performance envelopes with pulse repetition rate as the controlled parameter. This study [50] considered a *6.4* mm diameter wire inside a *254* mm diameter tube containing air at STP with a *20* GΩm flyash. In addition, the back ion current ratio α is shown, in order to give a measure of the intensity of back corona.

It is clear that back corona has a devastating effect on particle charge and this degradation reduces drastically the particle migration velocity. Once back corona is initiated in the dust layer, pulsed energization can do little to ameliorate the devastating particle discharging effect of the positive ions emitted by the layer. It should also be noted that α values as low as *0.002* produce significant degradation in performance. Such low proportions of back flux would not be detected by ESP terminal electrical behavior.

4.5 Consequences of Pulsing Effects on ESP Operation

A valid basis for comparison of ESP performance under different powering schemes is mean terminal current.

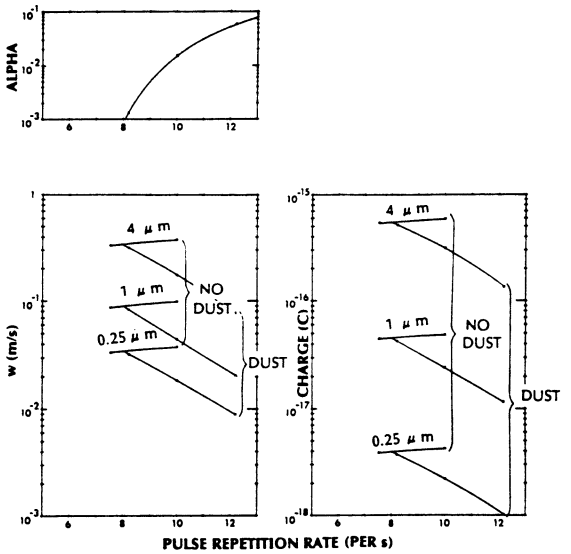

Fig. 10: Parameter performance envelope for 56+60 kV, 800 μs pulses. 6.35 mm wire, 254 mm tube 3 m long, 293 K air with 1.5 m/s core velocity.

The adopted back corona model has anode current density as the only electrically controllable variable to determine the back corona level. When back corona is absent, increases in powering voltage levels, pulse widths, repetition rates and peak values all improve ESP efficiency, while also increasing ESP current. The limit to increased current is the onset of back corona.

Modeling studies show that when back corona is absent, pulsed energization produces worse ESP efficiencies than dc operation at the same current. Pulsing however permits back corona free operation under some conditions of very high dust resistivity, where this cannot be achieved with dc.

Some reported field studies of pulsed precipitation [14,61] have been carried out with pulsing superimposed on a base energization level above the ESP corona inception, so that the corona continued in the interpulse period. Modeling studies [40] show that the low (*10* to *100* pps) repetition rates lead to negligible change in mean current. Therefore, if back corona was present in the pure dc case, no improvement can be found in this pulsing mode.

There is a practical minimum anode current density for dc energization which is around *50* μ A/m^2 for typical ESP dimensions (*2.8* mm (0.11 in) diameter wire and *0.2* m (8 in) duct). When extremely high resistivity flyash is encountered, the dc voltage cannot be adjusted to produce low enough operating currents to avoid back corona. In these cases, pulsed energization is advantageous in a mode of operation with a quiescent voltage level (between pulses) below corona inception, so that corona is generated only at the pulsing rate of *10* to *100* pps. In this case, it is possible to reduce the mean current to much lower values, permitting avoidance of back corona. ESP performance with such pulsing and high resistivity flyash is not as good as with dc and a low resistivity flyash in an ESP of the same size. This is because of the necessity of preserving a sub-inception quiescent voltage in the long interpulse period, which limits the particle migration field. On the other hand with dc operation, the mean cathode voltage is higher and there is always a significant field distortion due to drifting negative ions: both these factors increase the migration field significantly over the pulsed case. The effect of reduced migration field dominates any particle charge enhancements with pulsed energization.

Since the sub-inception quiescent field profile limits pulsed ESP performance, one option is to raise the sub-inception field profile by using a larger diameter wire. The ESP inception voltage rises, which for dc powering presents a problem past a certain diameter by reducing the dc operating voltage range that is limited by the inception and sparkover voltages. However with pulsed powering, ESP current is not controlled by adjustment of the quiescent voltage, but by other means (such as repetition rate control) and the benefits of a thicker wire can be seen by comparing Figs. 11 and 12. (It should be noted that this study

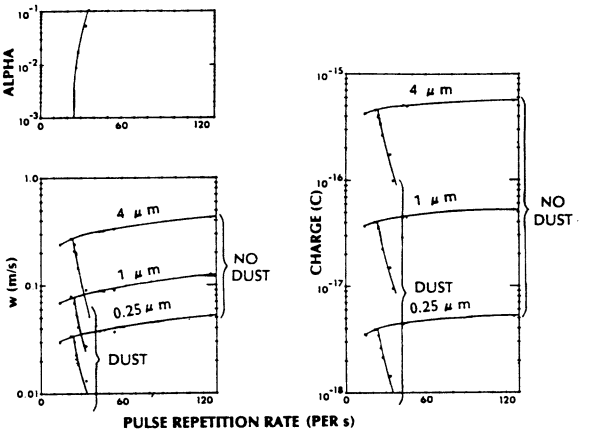

Fig. 11: Parameter performance envelope for 56+60 kV, 200 μs pulses. 6.35 mm wire, 254 mm tube 3 m long, 293 K air with 1.5 m/s core velocity.

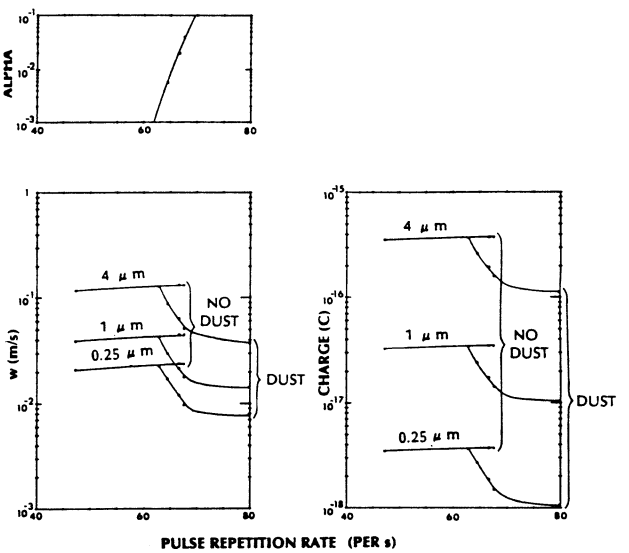

Fig. 12: Parameter performance envelope for 39+30 kV, 200 μs pulses. 3.18 mm wire, 254 mm tube 3 m long, 293 K air with 1.5 m/s core velocity.

was carried out with no account taken of sparkover limits). The optimal migration velocities for *0.25*, *1*, and *4* μm particles with a *3.2* mm wire are *2.4*, *4.3*, and *14* cm/s, respectively, while with a *6.4* mm wire they are *3.4*, *7.7*, and *27* cm/s. The doubling of migration velocity for particles larger than *1* μm indicates a dramatic enhancement in ESP performance.

4.6 Selection of Pulse Parameters

Many different authors have expressed various opinions on which pulse parameters are significant, and what values they should take. At times these opinions appear to have been colored by the capabilities of the pulsing systems under study, with virtues being made of design limitations. The results of model studies serve to clarify the sensitivities of ESP performance to pulse parameters.

An initial study was limited to sinusoidal pulses, the generic waveform to be expected from the capacitor-switch-pulse transformer types of ESP pulsing power supplies discussed in the literature [2,62]. For study purposes, a *0.254* m diameter, *3* m long ESP was considered, operating with air at ambient conditions and mean speed of *1.5* m/s. Wires of *3.2* and *6.4* mm diameter were simulated. As in previous studies, sparkover limitations were not treated.

Figs. 10 and 11 present the effects of pulse width on particle migration velocity. It can be seen that the long *800* μs pulse yields significantly better behavior than the medium *200* μs pulse. As discussed previously, only for long pulses does the pulse width have important effects.

Figs. 11 and 13 show the performance envelopes for *200* μs pulses of two different amplitudes. The higher pulse enhances the peak migration velocities, more so

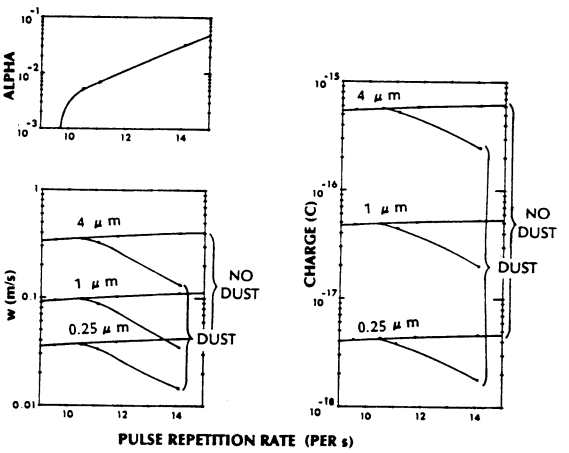

Fig. 13: Parameter performance envelope for 56+120 kV, 200 μs pulses, 6.35 mm wire, 254 mm tube 3 m long, 293 K air with 1.5 m/s core velocity.

for larger particles. The performance envelopes show the effects of pulse repetition rate variation, which is clearly a useful way of tuning the ESP current.

Some exploratory work has been carried out on pulse shape variation. One possibility shown in Fig. 14(a) is to prolong the falling edge of a sinusoidal pulse

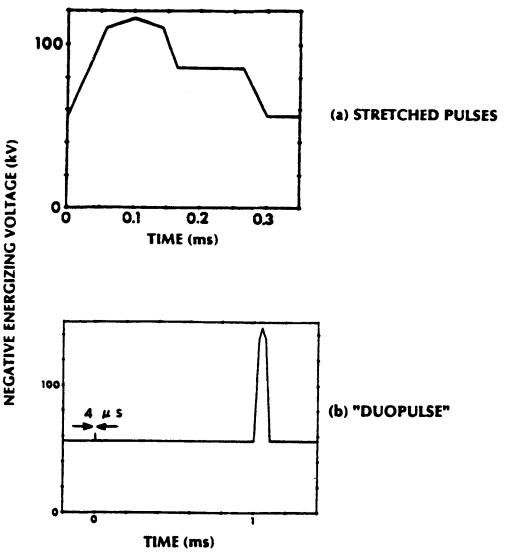

Fig. 14: Modified pulse shape strategies.

to increase the ESP field, but to limit the stretching so as not to permit any further ionization. Fig. 14(b) demonstrates a "duopulse" strategy, where a short pulse generates one Trichel ionization burst which then drifts well into the gas space. After *1* ms, a second very high, medium length, *100* μs pulse follows to raise the field and enhance charging by the first ion swarm. The results are summarized in Table 1 where they are compared with comparable dc (for duopulse) and sinusoid energization. The behavior is seen to depend on size and the presence of back corona. Without back corona, the plateau waveform boosted w for all particle sizes, but in the presence of back corona the gains were eliminated. The "duopulse" strategy benefited larger particles but in fact decreased *0.25* μm particle migration. It should also be noted in passing that the comparison between dc and sinusoid at *431* $\mu A/m^2$ shows the superior performance of dc at the same current level.

4.7 Ion Dynamics Near Wire and Reabsorption

One hitherto unreported phenomenon discovered in these model studies is the reabsorption of negative charge by the wire. With shorter pulses, the space charge distorted field may reverse at the wire surface after the pulse peak, and drive some negative charge back to the wire. This has been obtained with a *100* ns sinusoid pulse where electrons were reabsorbed, and also with *50* μs pulses in the ESP configuration of the previous section, where some of the negative ion swarm returned to the wire.

Such reabsorption could be utilized in very low back corona threshold dust situations (i.e., extremely high resistivity dusts), where another method of limiting the current density in addition to pulse repetition rate reduction may be necessary. Reabsorption might reduce the ionization from one energization pulse to less than 10% of one Trichel pulse. To examine reabsorption further, the pulse of Fig. 15 was applied to the model ESP with 3.2 mm wire. Fig. 16 illustrates the movement of negative ions back to the wire, and 47% of the ion swarm was reabsorbed in *100* μs.

Table 1

Effects and limits of pulse parameter variations.

Pulse Parameter	Effect of Increase in Parameter on Migration Velocity and Efficiency	Size Specificity of Effect	Limit to Parameter Increase
pedestal voltage	increase	all sizes equally	corona wire inception voltage
height	increase	all sizes equally	sparkover voltage
width	modest increase	better for medium and large particles	pulse interval increases to same magnitude as dust layer time constant
repetition rate	increase	all sizes equally	dust layer back corona threshold current

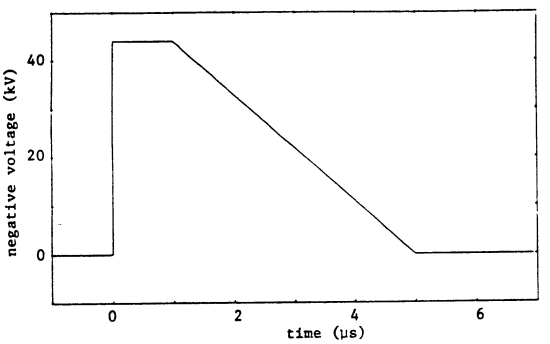

Fig. 15: Applied voltage pulse to produce negative ion reabsorption.

4.8 Discussion

The utility of a comprehensive simulation suite for the study of pulsed precipitation has been clearly shown. The complexity of modeling the Trichel pulse corona has yielded benefits in being able to confidently predict the time-varying generation of ionization in the ESP. Almost all previous ESP models have avoided this issue, but as a consequence are unable to address pulsed energization in any meaningful way.

It is now clear that the usefulness of pulsing lies in permitting low-current ESP operation when back corona due to high flyash resistivity precludes operation with dc energization. It is also clear that pulsing does not yield much benefit at current levels high enough to cause back corona. Modeling is useful in predicting the sensitivity of ESP behavior to pulse parameter variations, with increasing pulse height and repetition rate producing improved collection. Performance is insensitive to the specific width of medium pulses, but with long pulses width does improve collection (however, reabsorption may be significant for shorter pulses). Some flexibility is also apparent to tailor pulse shapes to optimize performance within the constraint of avoiding back corona.

Since back corona is such a significant factor in justifying pulsed energization and in providing a major constraint to the energization level, it should be recognized that the model of back corona is relatively unsophisticated. The model suite shows that ESP performance is very sensitive to relatively small levels of positive ion flux caused by back corona. Therefore, a more detailed representation of positive ion generation around the back corona threshold would enhance the power of the suite of models. The empirical, two linear segment model used is based on experimental measurements [57] which suggest that the inception of back corona is not as abrupt as modeled here. Additional experimental data, perhaps of a more refined nature, is required to support a model of positive ion injection more detailed around the back corona threshold.

Another important phenomenon that should be included in model studies is sparkover between electrodes, which defines the operating limit for most ESPs. Obviously some of the pulse amplitudes used in the above mentioned studies would be severely limited by flashover. Operating ESP experience generally leads the industry to believe that back corona promotes flashover at lower operating voltages, while pulsing permits higher peak voltages before flashover than is possible with dc. While a formative time lag effect is sometimes invoked to explain the increased peak voltage limits with pulsing, accepted breakdown time lags [63] are orders of magnitude faster than for instance the 250 μs pulse length used in [39]. While some results are available for the flashover limits of non-uniform gaps, these apply to quite different conditions from ESPs, and there is very little that extends to predicting behavior in the dusty, transient pulsed ESP environment. It is felt that the physics of sparkover is not understood sufficiently to justify at present a modeling effort analogous to the dynamic corona model described here. However, a well-controlled laboratory study of sparkover limits in the ESP environment may provide valuable empirical data that would be very beneficial for the ESP community.

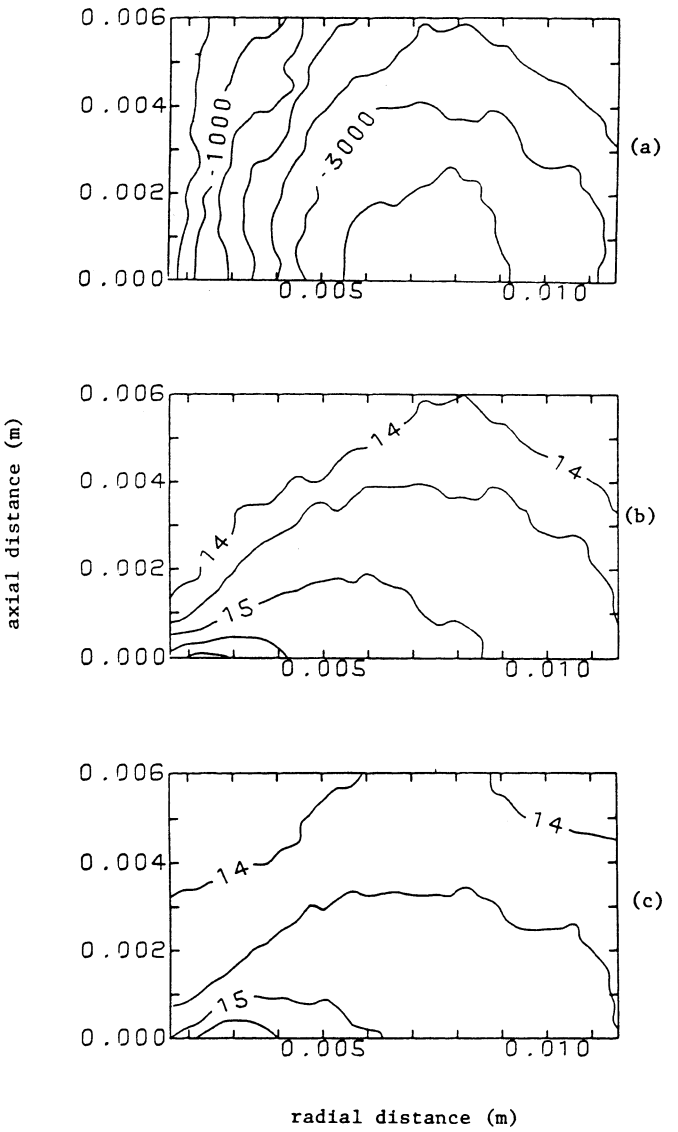

Fig. 16: Reabsorption of negative ions due to wire surface field reversal. 6.35 mm wire, 254 mm tube, 293 K air, phototuft extending z=-0.00035 to z=+0.00035 m. (a) Voltage profile at t=5 μs; (b) Negative ion density at t=5 μs, contour values are $\log(2\pi r N_n)$*; (c) Negative ion density at t=20 μs. Note that the contour line of 15 has moved closer to the cathode.*

5. PRECIPITATOR CONTROL

Operation of conventional ESPs at a fixed potential is not often desirable since changes in boiler operation or dust characteristics and loading will create variations in sparkover voltage. It is usually the case that efficiency is maximized by applying as large a potential as can be accommodated in the prevailing conditions without sparkover. This has traditionally been accomplished by controls which raise the wire voltage to achieve a specified spark rate and then back off by a given margin. The advent of thyristor controls for the transformer-rectifier (T-R) sets has permitted this type of control to respond much faster to changes in operating conditions. This allows a higher average power input without experiencing excessive sparking, which translates into an enhanced efficiency. This basic operating philosophy of most T-R controls does, however, carry a heavy penalty in power consumption. Since the annual cost of power consumed by a single *500* MW utility installation is typically about $100000, recent attempts have been made [64] to use opacity measurements in the stack gas to adjust the precipitator power input. In this way, some degree of optimization may be achieved while still providing compliance with emission requirements. This can be successful because of the nature of the opacity/power consumption curve [65] which saturates such that a *1%* increase in opacity can sometimes generate power savings of as much as 50% especially when lightly loaded. In this context it is also important to control a large ESP installation on a field-by-field basis.

5.1 *Control and Monitoring of Other Precipitator Functions*

Although a primary thrust in improving ESP performance has concentrated on the charging and migration aspects, it is nevertheless true that many existing units are deficient on account of secondary processes such as rapping reentrainment, sneakage, etc. as well as the result of poor aerodynamic design and corona wind which affects the turbulent diffusivity [66] discussed earlier. Computer-based control schemes have also been developed in an attempt to bring about improvements in these aspects. A good example of this may be found in the new generation of rapper control schemes [67]. Not only can the timing and sequence of rapping be adjusted to provide improvements, but also the rapping intensity can be adjusted in concert with flyash buildup in some schemes. Furthermore, it is also possible to reduce or remove the energization during rapping to affect the electrostatic forces holding the ash to the plates.

Increasing environmental and legislative pressure is also making it attractive to utilize such intelligent controllers for monitoring and recording purposes. By this means, performance can be continuously evaluated and alarms provided for operating conditions which are beyond preset limits. This is often extended to include hopper ash levels, T-R set operating parameters, gas flows, etc.

5.2 *Control of Pulsed Precipitators*

Intelligent control of conventional precipitators is currently limited by 2 problems:

(a) The lack of suitable sensors for measuring strategic parameters in situ.

(b) The limited number of control variables inherent in conventional precipitator applications.

Some aspects of the sensor issue are being addressed by recent work [68] aimed at diagnosing conditions within a working ESP by means of a biased bipolar current probe. In this way it is feasible to determine the ratios of the forward to back ion flux and make adjustments appropriately. Steps have to be taken to obviate some of the problems associated with the use of such probes in the precipitator environment. Currently this information is obtained in a laboratory experiment [57] or by calculation [69], but it is clear from the results presented earlier that the onset of back ion flux is a vital measure of precipitator operation. Similarly initiatives are being taken to develop

transducers to provide on-line information about the dust surface loading [70]. It is evident that the in situ resistivity is of paramount importance in controlling ESP performance. Although careful laboratory estimates can be made which properly allow for temperature and humidity effects [57], in situ values may vary considerably due to changes in packing factor as well as those due to fuel and boiler conditions. In situ resistivity measurement remains a challenge.

The use of pulse energization offers exciting opportunities for ESP control since, in principle, at least 4 independent electrical parameters are available for control instead of voltage alone as is conventionally the case. It is clear from Fig. 2 that not only is the pulse magnitude a controllable parameter, but the dc pedestal, the pulse width and pulse repetition rate are also available for control purposes. However, it has been shown earlier that the repetition frequency is much more effective at altering conditions than is the pulse width and, similarly, there are constraints on the choice of dc pedestal. Nevertheless, it is known that the value of the pedestal bias has important implications on the formation of corona tufts on the wire electrode under pulse conditions [42].

5.3 Parameter Performance Envelope Control

A major objective of the modeling effort described has been to provide the basis for the future development of control algorithms. The definition of "parameter performance envelopes" which specify optimum settings of the controlled variables in response to the prevailing measured ESP environment, provides the basis for precipitator management which takes advantage of the recent advances in thyristor control and the availability of inexpensive computing capabilities. The performance curves cannot be accurately derived entirely by modeling since some aspects are not amenable to calculation. However, it has been found possible by a combination of laboratory characterization, empirical correction, and off-line modeling in the temporal and spatial domain, to provide envelopes which can be used with actual utility ESPs [51]. The scheme outlined offers, in effect, an opportunity to undertake some limited tailoring of the performance of existing ESPs in response to fuel switching or changing operating conditions.

5.4 Strategy Development

The potential opportunities offered by pulse energization and advanced sensor development are not limited to maximizing efficiency such as shown in Figs. 10-13 and elsewhere [51]. As indicated previously, there is current utility interest in reducing power consumption so that algorithms based on the parameter performance envelopes could provide control which would "minimize power, subject to maintaining compliance". Similarly, there may be future legislative pressure to improve small particle capture which might provide another operating strategy, as mentioned previously.

The cost effectiveness of retrofitting pulsing is very dependent on individual circumstances. Generally, it is attractive for difficult situations with high-resistivity dust in units for which efficiency is not dominated by secondary effects. However, when pulse energization can be justified, the additional benefits provided by strategic control are likely to be attractive.

5.5 Second Generation Controllers

Model predictions indicate that some benefits accrue from changes in waveshape. For example, the "duopulse" strategy was shown to have benefits, but the additional hardware needed to implement such a scheme may outweigh the advantages. However, modeling such as that described, may reveal that other waveshapes produce even more favorable results. The case for the integration of rapping control into a pulse energization scheme is much stronger. Coordination of rapping and powering is already used with some conventional units and the additional ability to have some control over the distribution of electric field in the unit during rapping may provide some limited ability to generate electrical energization conditions which will limit rapping re-entrainment problems.

6. CONCLUSIONS

The need for performance improvements in both currently operating and future ESPs has been reviewed, and the severe restrictions placed on ESP efficiency by back corona have been discussed. The complex interacting processes contributing to ESP operation have been introduced together with a discussion of the mechanisms by which pulsed energization is hoped to improve ESP behavior.

Since other ESP models in use are steady-state, they are fundamentally unable to address the benefits of pulsing. The requirements for modeling ESP behavior under pulsed energization have been discussed and a comprehensive computational model of pulsed energization has been outlined. The results of parametric studies using the model have been summarized and the implications for ESP pulsing strategy discussed. Pulsing is seen to be a practical method of suppressing back corona in high resistivity flyash layers. Examples have been presented of the model's capability to study sophisticated pulse shaping strategies, although currently available pulsing technology is not oriented towards such strategies. The phenomenon of negative charge reabsorption by a pulse energized corona wire has been introduced and its utilization discussed. The necessity for experimental data on back corona inception as well as flashover limits has been indicated, and future refinements of the pulsed precipitation model have been discussed.

A separate Section has been devoted to the discussion of the implementation of ESP pulser control in light of economic and environmental benefits. A methodology has been introduced for the utilization of pulsed ESP model results into intelligent pulsing controllers, where the results of off-line model studies are distilled into parameter performance envelopes, which are incorporated into on-line control. The development of transducers to enable the exploitation of the wide range of control strategy options presented by pulsing has been reviewed.

It is clear that continued study of pulsed energization using the methodology of computational modeling underpinned by experimental data can yield benefits of improved ESP operation by facilitating the design and evaluation of pulsing control strategies.

7. ACKNOWLEDGMENTS

The authors are grateful to New York ERDA and the Empire State Electrical Energy Research Corporation who have supported programs on precipitator technology at the Rensselaer Polytechnic Institute.

It is a pleasure to acknowledge many valuable interactions with R.J. Schwabe, R.W.L. Snaddon, K.A. Walsh of General Electric and G.I. Tardos of the City University of New York.

8. REFERENCES

[1] L.T. McEvoy, K.R. Parker and A. Russel-Jones, "The Collection of Fine Particulate in Power Plant Electrostatic Precipitators," Proc. 6th Symp. on Trans. and Util. of Part. Contr. Tech., Vol. 1, EPRI, p. 6-1, 1978.

[2] H.H. Petersen and P. Lausen, "Precipitator Energization Utilizing an Energy Conserving Pulse Generator," Proc. 2nd Symp. on Trans. and Util. of Part. Contr. Tech., pp. 352-368, 1982.

[3] G.B. Moslehi and S.A. Self, "Electromechanics of Particulate Layers," IEEE Trans. Ind. Appl., Vol. IA-20, pp. 1594-1607, 1984.

[4] H.J. White, "Industrial Electrostatic Precipitation," Addison-Wesley, 1963.

[5] H.H. Petersen, "New Trends in Electrostatic Precipitation," Trans. IEEE, Vol. IA-17, pp. 496-501, 1981.

[6] D.O. Heinrich, "Electrostatic Precipitator Collector Spacings Above 300 mm," Atmos. Environ., Vol. 13, pp. 1707-1711, 1979.

[7] D.H. Pontius, P.V. Bush and L.E. Sparks, "A New Precharger for Two-stage Electrostatic Precipitation of High Resistivity Duct," Conf. Record of 1st Symp. on Trans. and Util. of Part Contr. Tech., pp. 275-285, 1978.

[8] S. Masuda, S.A. Mizuno, H. Nakatani and K. Kawahasa, "Application of Boxer-Charger in Pulsed Electrostatic Precipitator," Proc. of IEEE/IAS Annual Meeting, pp. 900-911, 1980.

[9] J.S. Lagarias, J.R. McDonald and D.V. Giovanni, "Assessment of the Commercial Potential for the High Intensity Ionizer in the Electric Utility Industry," APCA Journal, Vol. 31, pp. 1221-1227, 1981.

[10] R.E. Cooke, "Sulphur Trioxide Conditioning," Symp. on Electrostatic Precipitators for the Control of Fine Particles, EPA 650/2-75-016, January, 1975.

[11] L.E. Sparks, G.H. Ramsey and R.E. Valentine, "Comparison of Electrostatic Precipitator Performance with Pulse and DC Energization," Int. Conf. on Electrostatic Precipitation, Monterey, CA, 1981.

[12] J.F. Shoup and T. Lugar, "High Voltage Thyristors Used in Precipitators," Control Eng., pp. 129-136, 1981.

[13] W. Puille, L.E. Sparks, G.H. Marchant, Jr., and J.P. Gooch, "Evaluation of Performance Enhancement Obtained with Pulse Energization Systems on Hot Side Electrostatic Precipitators," Proc. 2nd Symp. on Trans. and Util. of Part. Contr. Tech., EPA Report, 1981.

[14] H.R. Osmers, "Pulse Energization Electrostatic Precipitation," ESEERCO Research Report #EP83-5, 1985.

[15] Anon., "Pulse Energization System Improves Performance at Carolina P and L," Electric Light and Power, 1981.

[16] C.A. Gallaer, "Electrostatic Precipitator Reference Manual," EPRI Research Report 1402-4, pp. 2.19-2.21, 1985.

[17] G.B. Nichols, "Particulate Matter Control - The Rapidly Advancing Technology," Proc. 6th Symp. on Trans. and Util. of Part. Contr. Tech., Vol. 1, EPRI, p. P-1, 1986.

[18] F.W. Peek, Jr., "Dielectric Phenomena in High-Voltage Engineering," McGraw-Hill, New York, 1929.

[19] H.I. Milde, "Pulse Corona Discharge in Electrostatic Precipitators," IEEE Trans., EI-17, pp. 179-186, 1982.

[20] G.W. Trichel, "The Mechanism of the Negative Point to Plane Corona Near Onset," Phys. Rev. 54(12), pp. 1078-1084, 1938.

[21] T. Ushita, N. Ikuta and M. Yatsuzuka, "Negative Pulse Coronas in Air," Elec. Eng. Japan, Vol. 88, pp. 45-52, January 1968.

[22] R. Morrow, "Theory of Negative Corona in Oxygen," Phys. Rev., Vol. A 32, pp. 1799-1809, 1985.

[23] R.S. Sigmond, "The Unipolar Corona Space Charge Flow Problem," J. Electrostatics, Vol. 18, pp. 249-272, 1986.

[24] M. Zahn, Electromagnetic Field Theory, Wiley, New York, 1979.

[25] A. Mizuno, "Review of Particle Charging Research," Proc. Int. Conf. on Electrostatic Precipitation, Monterey, CA, 14-16, October 1981, APCA, Pittsburgh, 1981.

[26] J.B. Smith and J.R. McDonald, "Development of a Theory for the Charging of Particles by Unipolar Ions," J. Aerosol Sci., Vol. 7, pp. 151-166, 1976.

[27] G.W. Hewitt, "The Charging of Small Particles for Electrostatic Precipitation," AIEE, Vol. 76-1, pp. 300-306, 1957.

[28] L. Salasoo, J.K. Nelson, R.J. Schwabe and R.W.L. Snaddon, "Estimation of Particulate Charging and Migration for Pulsed Precipitator Applications," J. Electrostatics, Vol. 19, pp. 1-19, 1987.

[29] E.C. Potter, "Electrostatic Precipitation Technology: A Different Viewpoint," APCA Journal, Vol. 28, pp. 40-46, 1978.

[30] K.J. McLean, "Factors Affecting the Resistivity of a Particulate Layer in Electrostatic Precipitators," APCA Journal, Vol. 26, pp. 866-870, September 1976.

[31] H.J. White, "Resistivity Problems in Electrostatic Precipitation," APCA Journal, Vol. 24, pp. 314-338, 1974.

[32] R.E. Bickelhaupt, "Electrical Volume Conduction in Flyash," APCA Journal, Vol. 24, pp. 251-255, 1974.

[33] R.E. Bickelhaupt, "Surface Resistivity and the Chemical Composition of Flyash," APCA Journal, Vol. 25, pp. 148-152, 1975.

[34] P.A. Lawless, "Progress in Modeling Back Corona," Proc. Symp. on the Transfer and Utilization of Particulate Control Technology, Denver CO, 24-28 July 1978, US EPA-600/7-79-044a, pp. 35-43 (Industrial Environmental Research Laboratory, EPA, Research Triangle Park NC, 1979)

[35] S. Masuda, "Back Discharge Phenomena in Electrostatic Precipitators," Proc. Symp. on the Transfer and Utilization of Particulate Control Technology, Denver CO, 24-28 July 1978, US EPA-600/7-79-044a, pp. 321-333.

[36] H.J. Hall, "Design and Application of High Voltage Power Supplies to Electrostatic Precipitators," APCA Journal, Vol. 25, pp. 132-138, 1975.

[37] L.C. Thanh, "Negative Corona in a Multiple Interacting Point-to-Plane Gap in Air," Conf. Rec. IAS 15th Ann. Mtg. Cincinnati 1980, pp. 1087-1092, IEEE, Piscataway 1980.

[38] P. Bayle and B. Cornebois, "Propagation of Ionizing Election Shock Waves in Electrical Breakdown," Phys. Rev., Vol. A 31, pp. 1046-1058, 1985.

[39] T.W. Lugar, J.H. Brummer and T.W. Rosch, "The Dynamic Response of Precipitator Performance to Pulse Powering," ASME-IEEE Joint Power Conf., Milwaukee, October 1985.

[40] G.I. Tardos, R.W.L. Snaddon, R.J. Schwabe, K.A. Walsh, L. Salasoo and J.K. Nelson, "A Study of Pulsed Energized Particle Collection in a Bench Scale Electrostatic Precipitator," J. Appl. Phys.,Vol. 62, pp. 2626-2632, 1987.

[41] J.L. DuBard, J.R. McDonald and L.E. Sparks, "First Measurements of Aerosol Particle Charging by Free Electrons - A Preliminary Report," J. Aerosol Sci., Vol. 14, pp. 5-10, 1983.

[42] R.J. Schwabe, R.W.L. Snaddon, J.K. Nelson and L. Salasoo, "An Optical Study of Negative Corona Tuft Distribution for Pulsed Precipitator Applications," submitted to J. Phys. D.

[43] J.R. McDonald, W.B. Smith, H.W. Spencer, III and L.E. Sparks, "A Mathematical Model for Calculating Electrical Conditions in Wire-Duct Electrostatic Precipitation Devices," J. Appl. Phys., Vol. 48, pp. 2231-2242, 1977.

[44] A.J. Davies and C.J. Evans, "Field Distortion in Gaseous Discharges Between Parallel-Plate Electrodes," Proc. IEE, Vol. 114, pp. 1547-1550, 1967.

[45] A.J. Davies and C.J. Evans, "Computer Simulation of Rapidly Developing Gaseous Discharges," Proc. IEE, Vol. 118, pp. 816-823, 1971.

[46] A.J. Davies, C.J. Evans and P.M. Woodison, "Computation of Ionization Growth at High Current Densities," Proc. IEE, Vol. 122, pp. 765-768, 1975.

[47] A.J. Davies, C.J. Evans, P. Townsend and P.M. Woodison, "Computation of Axial and Radial Development of Discharges Between Plane Parallel Electrodes," Proc. IEE, Vol. 124, pp. 179-182, 1977.

[48] L.N. Menegozzi and P.L. Feldman, "The Physics of Pulse Energization of Electrostatic Precipitators," presented at 3rd Symp. on the Transfer and Utilization of Particulate Control Technology, Orlando FL, 9-13 March 1981.

[49] New York State Energy Research and Development Authority, "Pulsed Electrostatic Precipitation", Final Contract Report No. 600-FFES-ES-84, Albany, 1984.

[50] L. Salasoo, "Pulsed Electrostatic Precipitation", Ph.D. RPI, University Microfilms, Ann Arbor, 1986.

[51] Empire State Electric Energy Research Corporation, "Pulsed Electrostatic Precipitation", Phase 2, Research Report EP84-35, New York. 1986.

[52] S. Masuda and A. Mizuno, "Maximum Charge of a Spherical Particle Imparted by Pulse Charging," in Charge Storage, Charge Transfer and Electrostatics with their Applications, ed. Y. Wada, Elsevier-Kodansha, Kyoto 1978.

[53] G. Leonard, M. Mitchner and S.A. Self, "Particle Transport in Electrostatic Precipitators," Atmospheric Environment, Vol. 14, pp. 1289-1299, 1980.

[54] J.R. McDonald, M.H. Anderson, R.H. Mosley and L.E. Sparks, "Charge Measurements on Individual Particles Exiting Laboratory Precipitators with Positive and Negative Corona at Various Temperatures," J. Appl. Phys., Vol. 51, pp. 3632-3643, 1980.

[55] G.I. Tardos, R.W.L. Snaddon and P.W. Dietz, "Electrical Charge Measurements on Fine Airborne Particles," Proc. IEEE IAS Ann. Mtg., pp. 1013-1018, Mexico City, October 1983.

[56] M. Durham, G. Rinard, D. Rugg and L.E. Sparks, "Measurement and Interpretation of Current Density Distribution and Charge/Mass Data," Proc. 3rd Symp. on the Transfer and Utilization of Particulate Control Technology, Orlando FL, March 1981, US EPA-600/9-82-005B, pp. 54-65, Industrial Environment Research Laboratory, EPA, Research Triangle Park, NC, 1982.

[57] R.W.L. Snaddon, R.J. Schwabe, K.A. Walsh, J.K. Nelson and L. Salasoo, "An Investigation of the Emission of Reverse Ion Current From Electrically Stressed Dust Layers," submitted to J. Electrostatics.

[58] P.A. Lawless and L.E. Sparks, "A Mathematical Model for Calculating Effects of Back Corona in Wire-Duct Electrostatic Precipitators," J. Appl. Phys., Vol. 51, pp. 242-256, 1980.

[59] W.M. Kays, Convective Heat and Mass Transfer, McGraw-Hill, New York, 1966.

[60] Empire State Electric Energy Research Corporation, "Pulser Applications Assessment for New York State Precipitator Installations", Research Report EP86-10, New York, 1987.

[61] Electric Power Research Institute, "An Investigation of Precipitator Pulse Energization", CS-4717, EPRI, Palo Alto, 1986.

[62] K. Porle, "Reduced Emission and Energy Consumption with Pulsed Energization of Electrostatic Precipitators," J. Electrostatics, Vol. 16, pp. 299-314, 1985.

[63] R.T. Waters in "Electrical Breakdown of Gases", ed. J.M. Meek and J.D. Craggs, Wiley, New York, 1978.

[64] J.J. Roosma and J.B. Howard, "Power Consumption of Opacity Feedback Controlled Electrostatic Precipitator Transformer-Rectifier," Proc. 6th Symp. Trans. and Util. Part. Contr. Tech., Vol. 2, EPRI, p. 26-1, 1986.

[65] D.L. Lueckenotte and V.L. Kunzweiler, "The Evaluation of Tests and the Economic Implications of Power Reduction of Electrostatic Precipitators," Proc. 6th Symp. Trans. and Util. Part. Contr. Tech., Vol. 2, EPRI, p. 24-1.

[66] G.J. Leonard, M. Mitchner and S.A. Self, "Experimental Study of the Effect of Turbulent Diffusion on Precipitator Efficiency," J. Aerosol Sci., Vol. 13, pp. 271-284, 1981.

[67] G.R. Gawreluk, M. Barav and S.R. Coco, "First Utility Application of a New Microprocessor-Based Distributed Control System for Electrostatic Precipitators," Proc. 6th Symp. Trans. and Util. Part. Contr. Tech., Vol. 2, EPRI, p. 25-1, 1986.

[68] S. Masuda and Y. Nonogaki, "Sensing of Back Discharge and Bipolar Ionic Current," J. Electrostatics, Vol. 10, p. 73, 1981.

[69] J.F. Hoburg, "Charge Density, Electric Field and Particle Charging in Electrostatic Precipitation with Back Ionization," Trans. IEEE, Vol. IA-18, pp. 666-672, 1982.

[70] S. Masuda, T. Itagaki, S. Hosokawa, "Diagnostic Technology of Precipitator Operation," Proc. 6th Symp. Trans. and Util. Part. Contr. Tech., Vol. 2, EPRI, p. 21-1, 1986.

Manuscript was received on 2 July 1987.